



Model-based estimation of the reaction forces in an elastic system supporting large-size crankshafts during measurements of their geometric quantities



Krzysztof Nozdrzykowski, Leszek Chybowski*, Lech Dorobczyński

Maritime University of Szczecin, ul. Waly Chrobrego 1-2, 70-500 Szczecin, Poland

ARTICLE INFO

Article history:

Received 11 September 2019
 Received in revised form 3 January 2020
 Accepted 22 January 2020
 Available online 25 January 2020

Keywords:

Geometry measurements
 Large-size crankshaft
 Elastic deflection
 Reaction forces
 Interpolating models

ABSTRACT

We have previously described a novel crankshaft support system that can be used when measuring and testing crankshafts. Here, we extend our studies on this system using mathematical models (basic polyharmonic, spline-based polyharmonic, and monoharmonic functions) to identify the optimal conditions for supporting geometric measurements of large crankshafts. The obtained results improved the accuracy of this system and provided alternative solutions by minimizing shaft deflection during measurements. It was proposed and confirmed that variable reaction forces in flexible crankshaft supports can be mapped using a monoharmonic model with a good fit to the source data. At various selected crankshaft positions, finite element analysis software was used to determine the reaction forces, for which three different mathematical models were tested. The usefulness of each individual model was discussed in terms of the complexity and accuracy of mapping the source values.

© 2020 The Author(s). Published by Elsevier Ltd. This is an open access article under the CC BY license (<http://creativecommons.org/licenses/by/4.0/>).

1. Introduction

The machinery and equipment used in ship engine rooms often contain large components that are characterized by low and variable rigidity and high susceptibility to flexural deformation. These components include the crankshafts of the power engine pistons of a ship's main propulsion, auxiliary machines, and generator sets [1]. These are mostly shafts of diesel piston power engines, commonly also used in other types of haulage and transport (rail, road), agriculture and industrial construction. As highlighted in the literature [2], when it comes to machining, crankshafts are the most labour-consuming engine components with the longest manufacturing cycle. Machining is difficult due to the complex shape of a shaft, its low rigidity, high requirements for geometric precision and surface roughness, as well as the necessity of balancing the shaft and the interoperational and final evaluation of a shaft's geometric condition.

The precision of a crankshaft's manufacture strongly affects the proper functioning of the crank-and-piston system and, hence, of the entire working machine. At the same time, it has been esti-

mated that crankshafts account for 20–25% of the cost of the entire machine [2].

For this type of machinery components, there are high requirements of the material [3–5] and of the geometric precision of the manufacturing process defined in the product specification [6,7]. For this reason, the modern production process requires continuous control of the quality of the manufactured surface. Full and accurate assessment of the geometric condition of the product can only be guaranteed if the appropriate measurement methods and techniques are used. These should be feasible in regard to metrology and apparatus; the accuracy of which must be adaptable to the tolerances given in the specification.

Current methods to assess the geometry of large shafts are limited to linear and angular measurements, including journal diameters, measurements of deflection of crank webs, assessing the condition of the top layer of journals and cranks, and surface roughness measurements. However, the above-mentioned procedures do not permit a complete and correct assessment of the intricate geometry of a shaft, mainly due to the elastic deformation caused by the assumed support conditions. Existing solutions do not guarantee accurate measurements due to errors resulting from elastic deformation during measurements [6,8].

In overhaul docks and repair workshops, reference measurement methods are often used to measure the deviation and shape contours of large and heavy crankshafts, with the measured object being fixed in V-blocks [9–14]. Reference methods are based on

* Corresponding author.

E-mail addresses: k.nozdrzykowski@am.szczecin.pl (K. Nozdrzykowski), l.chybowski@am.szczecin.pl (L. Chybowski), l.dorobczynski@am.szczecin.pl (L. Dorobczyński).

evaluating the position of the points of the measured profile in relation to one or more points of that profile. In shafts used in medium-speed engines (for generating sets, traction motors, etc.), four V-blocks are typically used for fixation, while for large shafts in slow-speed engines (rated speed below 450 rpm), more V-blocks are needed to fix and support the shaft [15,16]. In this case, the procedure is a series of separate measurements (mostly performed using universal measuring equipment) [17–19], which cover linear and angular dimensions and the radial and axial run-out (whip) of journals. In addition, a final criterion used to assess shaft geometry accuracy is measuring the deformation of crank webs, which is called a deflection measurement [20–22].

The measurement procedures of large-size crankshafts show significant gaps concerning comprehensive measurements of geometric deviation, i.e. those in both the shape and the position of the axes. They are based on measurements that have been used for many years and whose accuracy has not been updated to match the increasing manufacturing precision expected of modern crankshafts. These measures account for the presence of elastic deformation of the shaft, and thus web deflection measurements are necessary to determine whether the crankshaft is within acceptable workable limits.

Significant deficiencies in end-to-end measurements of geometric deviations in large crankshafts can especially be seen in their practical adaptation and their use in repair or overhaul facilities, such as repair docks or ship engine manufacturing plants [13,23]. A number of studies have shown that to accurately assess the geometric condition of a shaft, suitable measurement conditions are essential, including support conditions that eliminate any deflection and, consequently, any elastic deformation of the crankshaft under the influence of its own weight and those caused by its geometric deviation [24–26]. Elimination of this deflection is only possible if there is constant contact between the supports and the main journals of the shaft. Such conditions cannot be guaranteed by only supporting the shaft with a few selected main journals or with an uncontrolled set of rigid supports that maintain a fixed height position. Unintentional pre-deflection can occur in the position of the main journals, which generates elastic deformation

when the shaft rotates [27]. An example is shown in Fig. 1. This state causes the geometric deviation and elastic deformation, which are coupled with each other, to interact and the geometric evaluation of the shaft becomes unreliable.

To ensure correct measurement conditions, it is necessary to support the main journals of the shaft with a set of supports that compensate for its deflection and elastic deformation under the influence of its own weight as well as those caused by any geometric deviation of the shaft. The values of the reaction forces at the contact between the support heads and the main journals should guarantee zero deflection at the journals when rotating the supported shaft through a given angle [27].

2. Methods and materials

2.1. An innovative measuring methodology for evaluating the geometry of a flexibly supported shaft

This study aimed to improve the precision of methods for measuring the geometry of large-size crankshafts. The results, described herein, underpin the development of an innovative measurement methodology with a controllable exertion of reaction forces by the supports, based on the concept of the so-called flexible shaft support [25]. Fig. 2 shows a test rig constructed on the basis of the authors' concept of the measuring system, equipped with flexible support for the measured object. The idea of a flexible support was detailed in one of the authors' previous papers [27].

The use of flexible supports makes it possible, in practice, to eliminate any elastic deflection of a shaft. Regardless of the possible geometric deviation, the elastic supports, which exert pre-set reaction forces, act as flexible elements that compensate for any possible elastic deflection of the shaft. The purpose of the supports is to exert the pre-set reaction forces that guarantee zero deflection at the individual main journals. The required reaction forces at the contact of the support heads and journals are determined in advance for the selected shaft positions from the FEM strength calculations [26,28]. In addition, the elimination of the deflection on the main journals relieves the centres fixing the shaft. As a result,

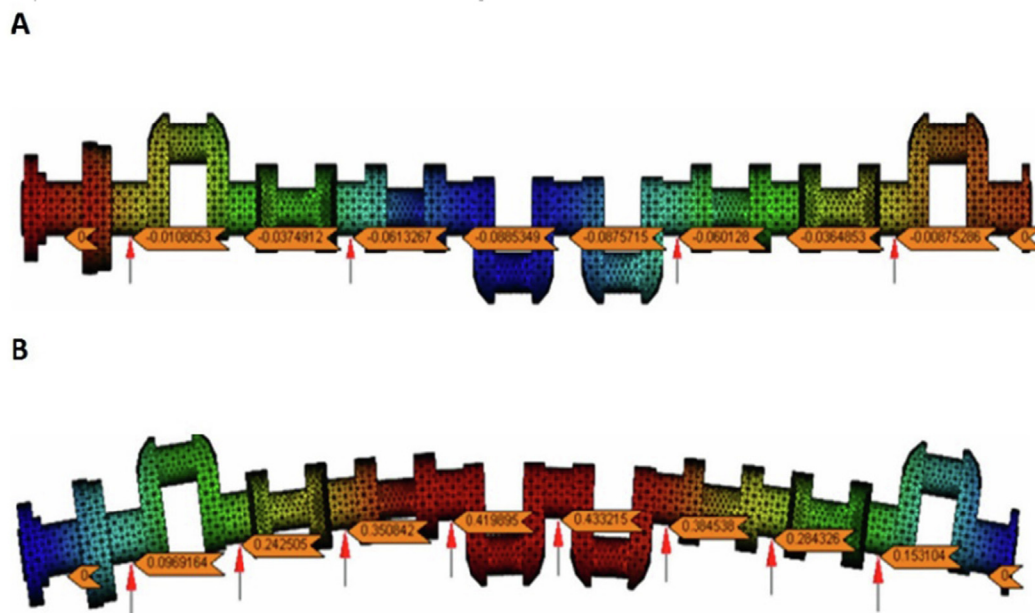


Fig. 1. Deflection in the center of the crankshaft, assuming zero deflection at the outermost journals [prepared by the authors based on Ref. [27]]; A – crankshaft resting on four rigid supports evenly spaced along the shaft; B – the shaft resting on eight supports loaded with a uniform reaction force of 1080.5 N ensuring zero deflection at the outermost journals.



Fig. 2. Prototype rig for measuring geometric deviation of large-size crankshafts during the measurement of a shaft of the Buckau-Wolf R8VD-136 engine.

the centres act as unloaded elements that securely retain the shaft. Measuring under these conditions corresponds to a non-reference scenario with the examined object being fixed in the centres. The axis determined by the centres is thereby a baseline for the measurements of the condition of the geometric shaft. This baseline is then used as the axis of reference for determining geometric deviation.

The elastic support system is made up of a set of elastic supports, the number, and arrangement of which depend on the number and arrangement of the main journals of the shaft. These V-block supports are self-adjusting, flexible and are the rolling-type. They do not limit the possible displacement of any main journals resulting from an inaccurately manufactured shaft. They exert a reactive force in order to eliminate shaft deflection, while at the same time they offset any possible displacement caused by any geometric deviation. The variable pressures and corresponding forces in the actuators of the relieving supports are continuously adjusted by means of precision proportional current-controlled reduction valves. Each flexible support exerts a force that depends on the crank angle. These forces are calculated in advance using the programs dedicated to strength analysis of machine components, implementing the finite element method, assuming zero deflection in the main journals of the shaft [29,30].

However, changing the value of the forces by adjusting the pressure of the medium that drives the relieving support actuators does not ensure that the required relieving forces are set unambiguously. The actual forces exerted by the pressure-controlled supports depend on a number of factors that determine the characteristics of the actuators themselves, such as resistance to friction, the type of medium, the shape of the actuator elements, the materials used and the actuator's structural design. Therefore, in the developed system, additional strain gauge force transducers were used that were situated between the heads and actuators of the flexible supports. In this way, the necessary force is the parameter that controls the pressure in the reduction valves. The pressure in the actuators of the flexible supports is thus controlled by the force and adjusted to the required relief force, determined using finite element analysis (FEA) software. The shaft's axial fixation is provided by a set of two ball-ended centres, one of which is stationary

and the other is resiliently mounted, parallel to the axis. This ensures that the shaft is in continuous contact with the locating centres, regardless of any elastic deformation in the shaft and that the centres automatically adjust the pressure they provide.

The measuring system is a trolley, equipped with a tripod and a measuring sensor, which moves along the guides parallel to the axis of the main journals of the shaft being measured. The system is equipped with shaft rotation control, which allows continuous data recording and transfers it to the computer's memory. The value of the reaction forces that eliminate elastic shaft deflection is pre-determined and then replaced by mathematical formulas. These forces are continuously monitored through precise, proportional current-controlled reduction valves, which cooperate in a feedback system with force sensors that measure the actual reaction forces at the contact points between the support heads and main journals. The computer checks the entire measurement process, regulates the values of the reaction forces, records the data and analyses the results.

2.2. Measurement procedure and a proposed improvement

This section provides a brief description of the measurement method. Detailed information regarding the concept of a flexible shaft support can be found in Ref. [27]. Assessing the geometric condition of large crankshafts using the developed measuring system consists of the following procedure:

1. **Determining the shaft fixing method.** It is possible to fix the shaft with the faces of centres or with two fixed V-blocks supporting the outermost main journals.
2. **Determining the basic parameters of the measuring system.** At this stage, the V-block opening angles, the trolley position, the measuring sensor and the sensor's stylus orientation relative to the measured outline are selected.
3. **Determining parameters of the shaft's flexible support system.** At this stage, the number of flexible V-block supports to be deployed is determined. The FEM methods are then used to determine the reaction forces to create the support conditions that are most favourable for the elimination of any shaft

deflection and elastic deformation. Due to the time-consuming FEM calculations, the values of the required reaction forces from all the flexible supports are determined for the selected angular shaft positions, e.g. every 15 angular degrees. The last step at this stage is the development of a mathematical model for the calculated values of the reaction forces, which will make it possible to exert and continuously monitor the changes in the reaction forces when the shaft rotates, for any angular position.

4. **Determining the kinematic parameters of the measurement process.** This stage determines the shaft's required angular speed during measurement and the sampling rate of the measuring system.
5. **Collecting the data.** This is an essential stage in the measurement procedure, in which measurements are made according to the predefined plan. The results of the measurements are recorded by a data acquisition computer system.
6. **Processing measurement data and drawing conclusions.** This stage is computer-aided and consists of:
 - selection of the reference elements for the estimation of the geometric deviation being sought,
 - determination of the geometric deviation being sought (harmonic analysis of the roundness profiles; presentation of the measured profiles on graphs in the Cartesian and polar coordinate system and as a discrete amplitude spectrum; presentation of the relative positions of the cylindrical surface arrangement in a graphical form on a 3D graph),
 - statistical data processing, estimation of the errors,
 - the last step, which is to print the measurement report on the geometric condition of the crankshaft and to draw conclusions.

FEA software can calculate the theoretical forces for any angular position of the shaft. Therefore, these calculations can be performed when the crank angle (CA) is increased by a constant value, between 0° and 360°, which is a full rotation. However, the intensity of the calculations increases considerably as the angle graduation interval is shortened and, in practice, a reasonable angle step, e.g. 15°CA, must be adopted for individual measurements [31,32]. For intermediate shaft positions, the values of the reaction forces are based on the adopted mathematical model. As a result of testing the prototype unit, the authors have established that the efficiency of the presented measurement procedure can be improved by automating the mathematical model's development process. This model represents the changes in the reaction forces at the flexible supports when the shaft rotates. Therefore, the authors undertook to develop a relatively simple model with a high mapping accuracy.

It was hypothesized that a monoharmonic model would provide a precise mapping of the calculated forces. The authors assumed in this study that a good fit will be provided by a function with a determination coefficient $R^2 > 0.99$. To test this hypothesis, it was necessary to develop polyharmonic models, refine them to spline-based polyharmonic models, and then determine the dominant harmonic that was necessary to develop a monoharmonic model. The results were verified by determining the accuracy of the model's fitting to the initial data and calculating the maximum relative percentage error.

2.3. Data and assumptions of the analysis

Analysis was carried out using a steel crankshaft of a Buckau-Wolf R8VD-136 Engine. The view of the engine is shown in Fig. 3 and its basic specifications and the crankshaft specifications are given in Appendix 1 (Table A1,A2)

Table 1 shows examples of the reaction forces determined for the tested object, which was the above-mentioned crankshaft of the medium-speed engine of a ship's main propulsion unit. They were calculated using the FEA theory implemented in Midas NFX 2019 R1 (MSC Software Corporation, Newport Beach, CA, USA).

The results are presented graphically and were comprehensively analyzed. The findings showed that the distribution of the zero-deflection forces at the individual journals, in the interval of 0–360°CA, presented in the polar coordinate system, is approximately an ellipse (if magnified, it appears slightly deformed and resembling the number eight). This corresponds to a sinusoid-like function in the Cartesian coordinate system. According to the interpolation theory, the models used in the harmonic analysis of signals may be used to describe these characteristics [7,12,33–35]. The $R(\varphi)$ reaction force at the support can thus be given in general terms as the function:

$$R(\varphi) = R_0 + \sum_{n=1}^k A_{Rn} \cos n\varphi + \sum_{n=1}^k B_{Rn} \sin n\varphi \quad (1)$$

where: A_{Rn}, B_{Rn} – components of the amplitudes (N) of the consecutive n th harmonics of the reaction forces. k – the number of harmonics adopted in the analysis; n – the number of the subsequent harmonic; R_0 – the averaged reaction force for a full rotation of the shaft (N); φ – the angular position of the shaft (°CA).

The components of the individual harmonics are given as the following relationships, commonly used in numerical calculations [12]:

$$A_{Rn} = \frac{2}{n_j} \sum_{j=1}^{n_j} r_j \cos n \frac{2\pi j}{n_j} \quad (2)$$

$$B_{Rn} = \frac{2}{n_j} \sum_{j=1}^{n_j} r_j \sin n \frac{2\pi j}{n_j} \quad (3)$$

where: n_j – the number of intervals adopted for discretisation; r_j – the discretised values of the function $\Delta R(\varphi)$;

The Eq. (1) can also be written as:

$$R(\varphi) = R_0 + \sum_{n=1}^k C_{Rn} \sin(n\varphi + \varphi_{Rn}) \quad (4)$$

where: R_0 – the averaged, calculated reaction force for a full rotation of the shaft, C_{Rn} – the amplitude of the n -th harmonic of the function of the changes in the reaction forces, φ_{Rn} – the phase shift of the n -th harmonic of the function of the changes in the reaction forces.

The amplitudes C_{Rn} of the individual harmonics and their phase shifts are described by the following equations:

$$C_{Rn} = \sqrt{A_{Rn}^2 + B_{Rn}^2} \quad (5)$$

$$\operatorname{tgn} \varphi_{Rn} = \frac{B_{Rn}}{A_{Rn}} \quad (6)$$

In this analysis, the polyharmonic model described by Eq. (4) was used as the initial model. Therefore, in the first step, the individual amplitude values and the initial phases for the first six harmonics were determined from the forces calculated from the FEA method, using fast Fourier transform (FFT) [36–38]. Estimated values of coefficients of the Fourier series expansion of periodic functions can be computed in Matlab 2019a (MathWorks, Natick, MA, USA) using the *fft* function [39]. The results of the *fft* function must be scaled (Appendices 2–4). A polyharmonic model was built from the obtained amplitudes and phases of individual harmonics. The implementation of the algorithm in the Matlab R2019a environment was presented in Appendix 2 (code polyharmonic.m).

Next, in order to increase the model's accuracy in mapping the forces determined by the FEA program, an enhanced polyharmonic model, based on spline interpolation, was developed [40]. This type of interpolation is a numerical method involving the approximation of an unknown function with polynomials. For an interval $\langle a, b \rangle$ containing all $m + 1$ interpolation nodes, p subintervals are created: $\langle t_0, t_1 \rangle, \langle t_1, t_2 \rangle, \dots, \langle t_{p-1}, t_p \rangle$ such that $a = t_0 < t_1 < \dots < t_p = b$ and in each of them the function is interpolated with an interpolating polynomial (usually of low degree). The "merging" of these polynomials creates a spline. Spline S is a function that interpolates the function R if:

$$R(\varphi_i) = S(\varphi_i) \text{ dla } \varphi_i, i \in \{0, 1, \dots, m\} \quad (7)$$

where: φ_i – the interpolation node of the R function R .

In order to build a spline-based polyharmonic model, the spectrum was identified by the FFT method to determine the amplitudes and phases of the individual harmonics. This led to the development of a model with precise mapping. The implementation of the algorithm coded in the Matlab environment is shown in Appendix 3 (code splines.m).

Analyses of the amplitude spectra for polyharmonic models, presented later in this paper (Sections 3.1 and 3.2), has shown that the second harmonic is important for the mapping of data calculated from the FEA program. Therefore, it is recommended to use the monoharmonic function, as follows [41]:

$$R(\varphi) = R_0 + C_{R2} \sin(2\varphi + \varphi_{R2}) \quad (8)$$

where: C_{R2} – the amplitude of the 2nd harmonic of the function of the changes in the reaction forces; φ_{R2} – the phase shift of the 2nd harmonic of the function of the changes in the reaction forces.

Assuming that the reaction forces calculated from the FEA software at the support of a given journal for successive shaft positions:

$$\Phi_{FEA} = [\varphi_1, \varphi_2, \dots, \varphi_m] \quad (9)$$

are expressed in the form of a vector:

$$R_{FEA} = [R_1, R_2, \dots, R_m] \quad (10)$$

then, the individual elements of the Eq. (8) will be [41]:

$$R_0 = \frac{\sum_{i=1}^m R_i}{m} \quad (11)$$

$$C_{R2} = \frac{\max\{R_1, R_2, \dots, R_m\} - \min\{R_1, R_2, \dots, R_m\}}{2} \quad (12)$$

$$\varphi_{R2} = \arcsin\left(\frac{R_i - R_0}{C_{R2}}\right) - 2\varphi_i \quad (13)$$

where: φ_i – the angle, for which the phase shift is determined;

$$\frac{R_i - R_0}{C_{R2}} \in \langle -1, 1 \rangle$$

When determining phase shift, it is important that the variation of the model coincides with the variation of the curve, determined by connecting the points indicated by the FEA program. In other words, both characteristics should increase for a shaft position that corresponds to the angle of φ_i . For the determined values listed in Table 1, for even-numbered journals, $\varphi_i = 0^\circ\text{CA}$, and for odd-numbered journals, $\varphi_i = 45^\circ\text{CA}$, so this relationship takes the form [41]:

- for even-numbered journals:

$$\varphi_{R2} = \arcsin\left(\frac{R_i - R_0}{C_{R2}}\right) \quad (14)$$

- for odd-numbered journals:

$$\varphi_{R2} = \arcsin\left(\frac{R_i - R_0}{C_{R2}}\right) - \frac{\pi}{2} \quad (15)$$

The amplitudes and phase shifts of the individual harmonics were calculated using the Matlab environment. A sample code implementing the authors' algorithm is provided in Appendix 4 (code monoharmonic.m).

3. Results and discussion

3.1. Basic polyharmonic model

Initially, the polyharmonic model given by the Eq. (4) was analyzed. The amplitudes and phase shifts determined using FFT for the data listed in Table 1 are presented in Tables 2 and 3, respectively.

The determined amplitudes and phase shifts of the individual harmonics were used to build the basic polyharmonic model based on the Eq. (4). A comparison of the model with the values calculated using the FEA program, using journal no. 1 in the Cartesian and polar coordinate systems as an example, is shown in Figs. 4 and 5, respectively. The graphical presentation of the results shows a relatively poor fitting of the model to the results of the FEA calculations.

For the proposed model, indicators of its goodness-of-fit to the source data were determined. The values of the maximal relative error δ and the coefficient of determination R^2 for the proposed models are presented in Table 4.

The maximum relative error was nearly 15%, and the coefficient of determination for the worst-fitting journal no. 8 slightly exceeded 0.81. The function's goodness of fit did not satisfy the authors' conditions (it is less than 0.99). The poor fit of the model can be explained by the small number of interpolation nodes: $360^\circ\text{CA}/15^\circ\text{CA} = 24$. Accuracy of this model can be improved by increasing the number of points, e.g. doubling it (measurement every 7.5°CA), but this means doubling the calculation time with the FEA software. Another alternative is to increase the number of harmonics, but this would result in the additional complexity of the model, therefore, the requirement of the development of the simplest possible model would not be satisfied.

3.2. Spline-based polyharmonic model

In order to increase the function's goodness of fit to the data calculated using the FEA software, the authors carried out spline-interpolation for the data compiled in Table 3. The spectrum of such a characteristic can be determined with much greater precision than in the case described in Section 3.1, e.g. for data calculated with increments of 1°CA . For the presented case, the amplitudes and phase shifts determined by the FFT method for the data listed in Table 1 are presented in Tables 5 and 6, respectively.

The determined amplitudes and phase shifts of the individual harmonics were used to build the enhanced polyharmonic model (the spline-based polyharmonic function) given by Eqs. (4) and (7). A comparison of the model with the values calculated using the FEA program, on the example of journal no. 1 in the Cartesian and polar coordinate systems is shown in Figs. 6 and 7, respectively. The graphical presentation of the results gives a good illustration of the good fitting of the model to the results of the FEA calculations.

For the proposed spline-based polyharmonic model, the indicators of its goodness-of-fitting to the source data were determined.

Table 2
Amplitude values for the individual harmonics of the reaction forces in the polyharmonic model.

Journal no.	Harmonic						
	0	1	2	3	4	5	6
	Amplitude (N)						
1	778.23	5.14	53.18	4.21	1.86	1.17	0.87
2	885.68	11.52	123.94	10.29	4.76	3.12	2.37
3	992.42	14.53	178.20	16.59	8.32	5.77	4.55
4	1037.63	16.39	218.86	21.44	11.05	7.79	6.20
5	978.84	15.7	192.83	17.97	9.02	6.26	4.94
6	959.44	15.21	169.85	14.65	6.99	4.69	3.63
7	980.16	15.45	191.31	17.93	9.03	6.28	4.96
8	1023.74	15.38	209.84	20.78	10.77	7.61	6.07
9	1067.20	10.09	135.15	13.26	6.84	4.82	3.84
10	581.00	2.75	34.76	3.3	1.68	1.17	0.93

Table 3
Phase shifts for the individual harmonics of the reaction forces in the polyharmonic model.

Journal no.	Harmonic						
	0	1	2	3	4	5	6
	Phase ($^{\circ}$ CA)						
1	90.00	265.52	261.61	78.65	76.69	76.10	76.27
2	90.00	81.80	75.16	250.79	248.59	248.27	249.22
3	90.00	251.56	240.12	55.22	54.41	55.92	58.85
4	90.00	65.19	52.61	228.64	229.00	231.54	235.35
5	90.00	251.46	239.99	55.1	54.29	55.83	58.79
6	90.00	78.71	70.2	245.26	243.31	243.48	245.12
7	90.00	250.83	239.18	54.36	53.67	55.33	58.39
8	90.00	63.51	59.83	227.18	227.82	230.62	234.61
9	90.00	244.97	232.37	48.44	48.81	51.42	55.25
10	90.00	69.23	57.22	232.6	232.2	234.14	237.43

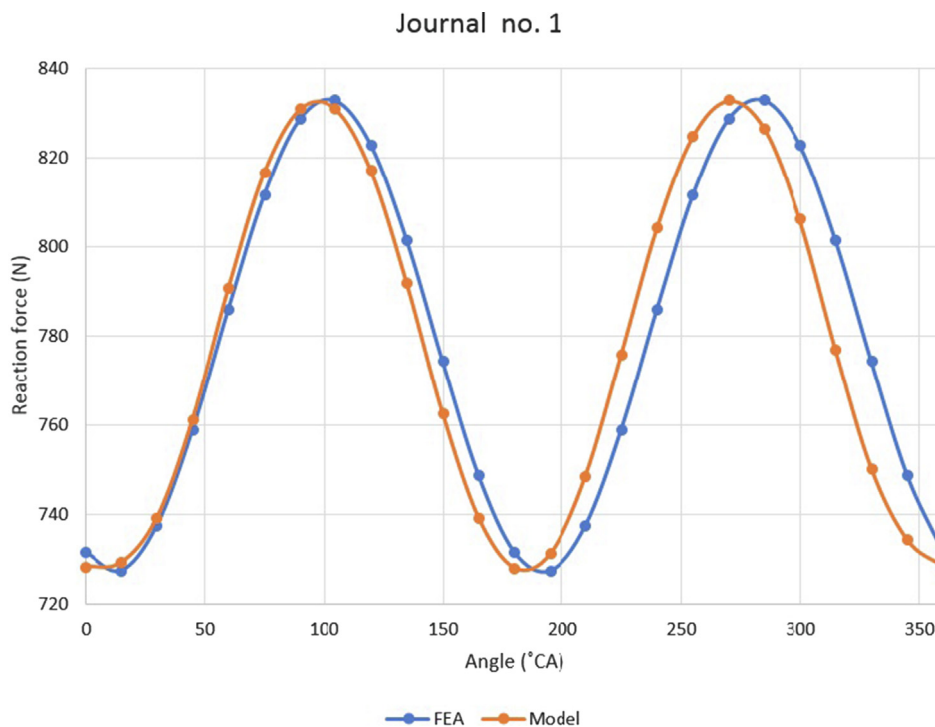


Fig. 4. Fit of the basic polyharmonic model to results obtained using the FEA calculation presented in Cartesian coordinates.

The values of the maximal relative error δ and the coefficient of determination R^2 for the proposed models are presented in Table 7.

The maximum relative error does not exceed 0.8% and the coefficient of determination is greater than 0.996. The fitting of the

function is therefore very good and meets the authors' criterion of $R^2 > 0.99$.

The disadvantage of this model is the need to use advanced numerical methods to determine the splines and to perform the

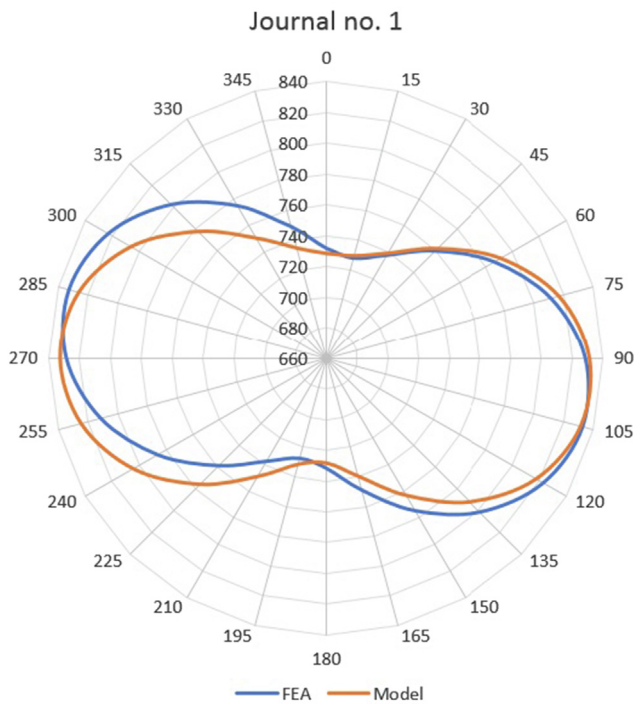


Fig. 5. Fit of the basic polyharmonic model to the results obtained using the FEA calculation presented in polar coordinates.

Table 4
The indicators for the fitting of the basic polyharmonic model.

Journal no.	δ (%)	R^2 (-)
1	3.09921	0.91971
2	6.85213	0.91745
3	8.60053	0.91331
4	11.73850	0.91208
5	9.41059	0.91325
6	8.83714	0.91594
7	9.29673	0.91313
8	14.9606	0.81513
9	6.09244	0.91205
10	3.09639	0.91275

Table 5
Amplitudes for the individual harmonics of the reaction forces in the spline-based polyharmonic model.

Journal no.	Harmonic						
	0	1	2	3	4	5	6
1	780.03	0.37	53.06	0.25	0.11	0.07	0.05
2	881.70	0.84	124.12	0.62	0.30	0.19	0.14
3	997.11	1.06	180.25	1.02	0.52	0.35	0.27
4	1032.65	1.20	222.53	1.23	0.69	0.48	0.37
5	983.91	1.15	195.07	1.10	0.56	0.38	0.29
6	954.27	1.11	170.64	0.89	0.43	0.29	0.21
7	985.12	1.13	193.65	1.10	0.56	0.39	0.29
8	1019.15	1.13	213.61	1.28	0.68	0.47	0.36
9	1070.26	0.74	137.44	0.82	0.43	0.30	0.23
10	580.13	0.20	35.23	0.20	0.10	0.07	0.06

FFT analysis. Therefore, it is necessary to use the appropriate software, which in this case is the Matlab environment.

3.3. Monoharmonic model

The authors' aim was to reduce the complexity of the model and to avoid performing complex numerical calculations such as the

Table 6
Phase shifts for the individual harmonics of the reaction forces in the spline-based polyharmonic model.

Journal no.	Harmonic						
	0	1	2	3	4	5	6
1	90.00	258.40	247.38	57.31	46.12	40.57	33.75
2	90.00	74.56	60.77	229.37	219.52	213.00	207.01
3	90.00	244.01	225.58	33.86	26.64	21.27	17.33
4	90.00	57.55	38.10	207.47	201.33	197.02	194.25
5	90.00	243.95	225.45	33.78	26.34	21.05	17.26
6	90.00	71.39	55.74	223.83	215.11	208.32	203.30
7	90.00	243.30	224.64	33.05	25.65	20.56	16.98
8	90.00	55.85	3635	206.05	200.01	196.14	193.48
9	90.00	237.33	217.87	27.28	20.78	16.89	14.11
10	90.00	61.67	42.68	211.33	204.14	199.45	196.20

spline interpolation and the use of FFT. To this end, the possibility of using a monoharmonic model given by Eq. (8) and whether it could give highly accurate results (R^2 should be greater than 0.99) was verified. For the case presented, the values of the amplitudes and phase shifts determined using the Eqs. (11)–(13) are presented in Table 8.

The determined values of the amplitudes and phase shifts were used to build a monoharmonic model (2nd-harmonic-based function) given by Eq. (8). A comparison of the model with the values calculated using the FEA program, on the example of journal no. 1 in the Cartesian and polar coordinate systems is shown in Figs. 8 and 9, respectively. As in the case of the spline-based polyharmonic model, the presentation of the obtained results also, in this case, gives a good illustration of the good fitting of the model to the FEA calculation results.

For the proposed monoharmonic model, the indicators of its goodness-of-fitting to the source data were determined. The values of the maximal relative error δ and the coefficient of determination R^2 for the proposed models are presented in Table 9.

The results of the model fitting analysis showed that the maximum relative error does not exceed 1.53% and the determination coefficient for all the journals is greater than 0.995. Therefore, the requirement of a high goodness-of-fit is satisfied. The proposed model is relatively simple, as it requires only three parameters to be determined for each journal. Moreover, in order to calculate these parameters, it is not necessary to use numerical analysis, to determine splines or to use FFT spectral analysis.

3.4. Models comparison

A comparison of the three models is given in Table 10. The maximum relative error δ_{max} and minimum determination factor R^2_{min} are shown for each function. The results indicate that the best fit was provided by the spline-based model, followed by the monoharmonic model, while the least accurate was the polyharmonic model. The monoharmonic model is the easiest to apply because it does not require a spectrum analysis to describe the individual harmonics of the force change function in reactions calculated using FEA software.

The data presented in Table 10 confirm the hypothesis that there is a monoharmonic model that ensures that the calculated forces are precisely mapped. This model is based on the 2nd harmonic of the function of reaction forces, which was determined using FEA software. Moreover, the proposed monoharmonic model provides a better fit to the source data than the basic polyharmonic model.

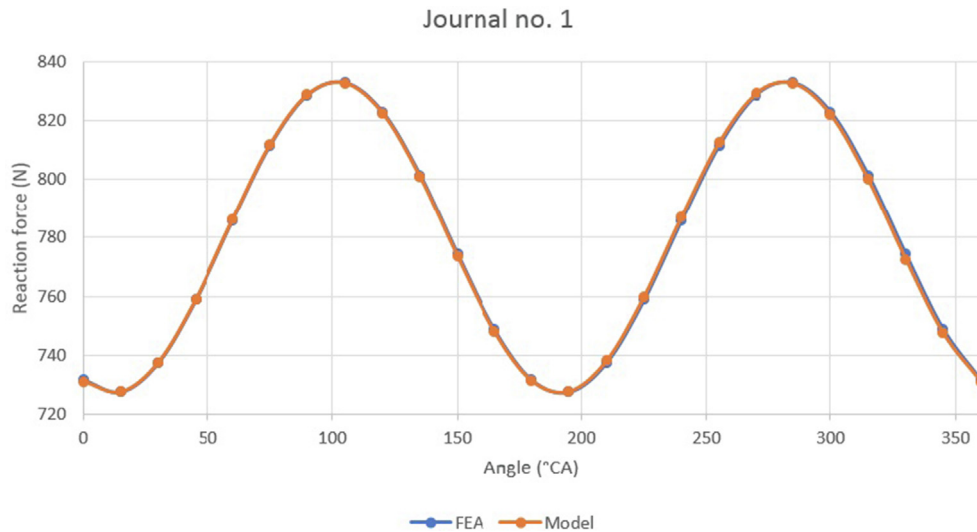


Fig. 6. Fitting the spline-based polyharmonic model to the results obtained using the FEA calculation presented in Cartesian coordinates.

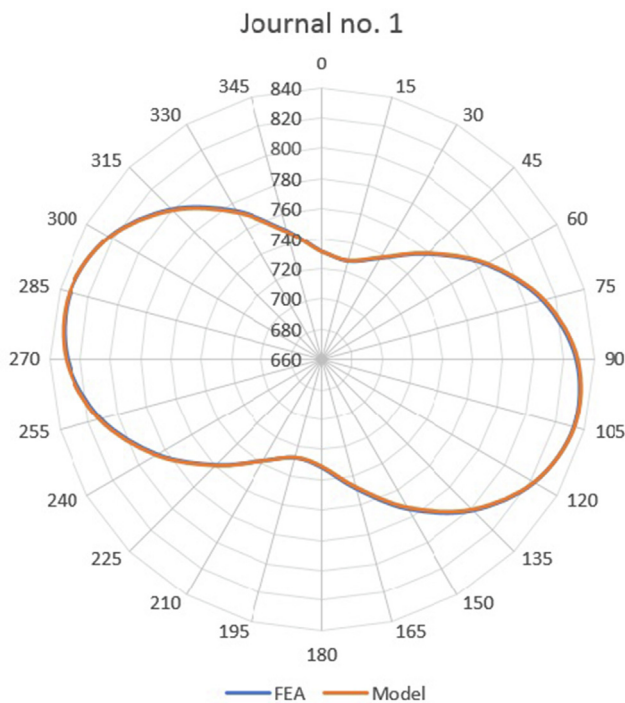


Fig. 7. Fitting the spline-based polyharmonic model to results obtained using the FEA calculation presented in polar coordinates.

4. Conclusions

Analyses of the test results showed unequivocally that the adopted apparatus was suitable for developing a mathematical model that is a record of the variation of reaction forces. One of the fundamental conditions necessary to ensure a shaft's actual geometric condition is assessed correctly is precisely monitoring these forces while measuring geometric deviations of the crankshafts. To this end, the proposed system, equipped with a flexible support system, can be used.

Both the spline-based polyharmonic model and the monoharmonic model provide the required mapping of the source data. The spline-based polyharmonic model is more accurate, but in

Table 7

The indicators for the fitting of the spline-based polyharmonic model.

Journal no.	δ (%)	R^2 (-)
1	0.22325	0.99603
2	0.46924	0.99959
3	0.57398	0.99956
4	0.74539	0.99956
5	0.63372	0.99956
6	0.61061	0.99957
7	0.62718	0.99956
8	0.33531	0.99989
9	0.40756	0.99955
10	0.20089	0.99956

Table 8

Values of the amplitudes and phase shifts for the monoharmonic model.

Journal no.	R_0 (N)	C_{R2} (N)	φ_{R2} (°CA)
1	778.23	52.69	-111.54
2	885.68	124.35	55.99
3	992.41	174.53	-135.05
4	1037.62	220.96	35.62
5	978.84	188.99	-135.16
6	959.44	169.82	51.86
7	980.16	188.27	-135.81
8	1023.73	212.82	33.83
9	1067.20	136.54	-141.47
10	581.00	34.52	40.59

order to implement it, requires more demanding computational power. For this reason, the monoharmonic model is a more attractive alternative.

Given the extremely good fit of the spline-based polyharmonic model and the monoharmonic model, it is reasonable to assume that a 15°CA angle is a reasonable angular increment to measure the geometry of the crankshaft's main journal.

The innovation of the approach described here lies in its ability to determine the reaction forces in supports at intermediate angular shaft positions, i.e. between the positions for which the values of reaction forces in supports are known from FEA analysis. This approach will enable the control of the supports using the FEA analysis data. Conducting FEA analyses for crankshaft positions determined using elevated density may yield more accurate results, but this will increase the calculation time. Future develop-

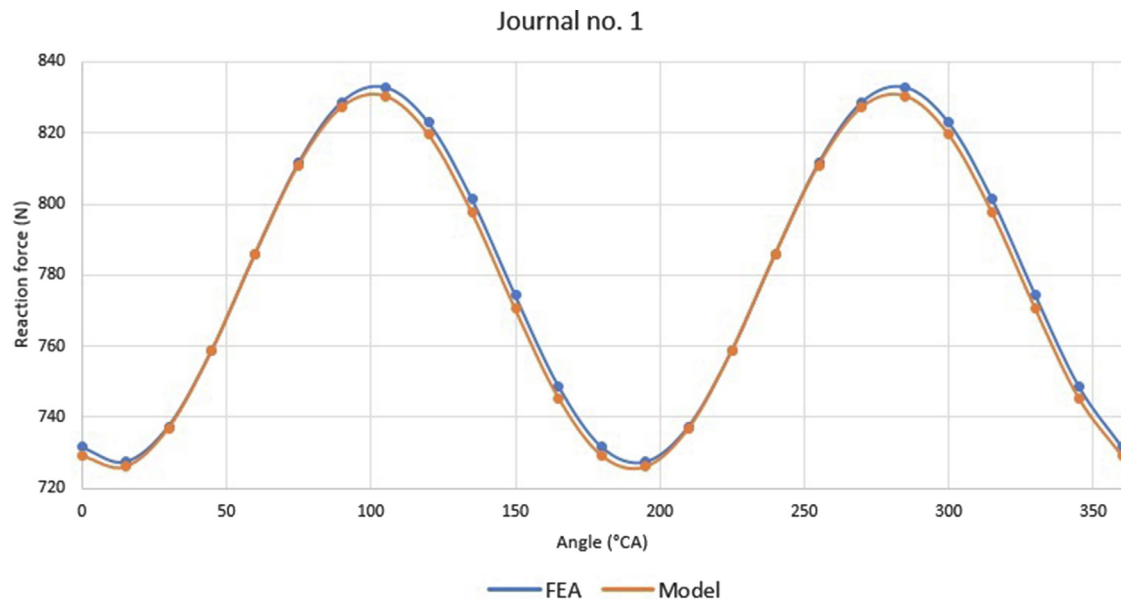


Fig. 8. Fitting the monoharmonic model to results obtained using the FEA calculation presented in Cartesian coordinates.

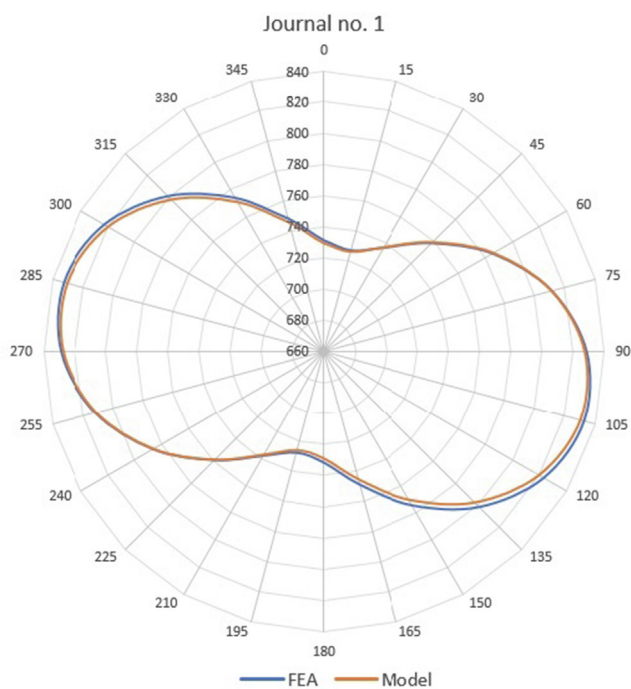


Fig. 9. Fitting the monoharmonic model to results obtained using the FEA calculation presented in polar coordinates.

ment of this measuring system includes using the data and the mathematical model by the computer-based automatic control for the crankshaft support. This may be developed based on the input data from the analyses carried out using the FEA software.

CRedit authorship contribution statement

Krzysztof Nozdrzykowski: Conceptualization, Methodology, Validation, Formal analysis, Investigation, Resources, Data curation, Writing - original draft, Writing - review & editing, Supervision, Project administration, Funding acquisition. **Leszek**

Table 9
Indicators for fitting the monoharmonic model.

Journal no.	δ (%)	R^2 (-)
1	0.49793	0.99868
2	1.39617	0.99594
3	0.93476	0.99993
4	1.19474	0.99938
5	1.00205	0.99993
6	1.52899	0.99767
7	0.94840	0.99988
8	1.10268	0.99934
9	0.68980	0.99906
10	0.33620	0.99968

Table 10
Accuracy comparison of analysed interpolation functions.

Model	δ_{max} (%)	R_{min}^2 (-)
Basic polyharmonic	14.9606	0.81513
Spline-based polyharmonic	0.74539	0.99603
Monoharmonic	1.52899	0.99594

Chybowski: Conceptualization, Methodology, Software, Validation, Formal analysis, Investigation, Resources, Data curation, Writing - original draft, Writing - review & editing, Visualization, Supervision, Project administration, Funding acquisition. **Lech Dorobczyński:** Conceptualization, Software, Formal analysis, Resources, Data curation, Writing - review & editing, Visualization.

Declaration of Competing Interest

The authors declare that they have no known competing financial interests or personal relationships that could have appeared to influence the work reported in this paper.

Acknowledgements

This research was co-funded by the Ministry of Science and Higher Education of Poland from Grant 1/S/IPNT/18 "Application

of the concept of flexible support in the measurement and assessment of the geometric condition of flaccid, large-size machine elements” and Grant 1/S/IESO/17 “Increasing the operational effectiveness of complex technical systems by systematic development and implementation of innovations using novel materials and modifying the object’s structure”.

Appendix

1. Basic data of the analysed crankshaft and the engine for which it was designed

Table A1

The basic specifications of the crankshaft of a Buckau-Wolf R8VD-136 engine.

Parameter	Description
Crankshaft length	3630 mm
Crankshaft weight	946.3 kg
Number of crank journals	8
Number of main journals	10
Crank journal diameter	144 mm
Main journal diameter	149 mm
Crank web dimensions	252 mm × 358 mm (oval)
Poison’s ratio of the material	0.3
Young’s modulus of the material	210 GPa

Table A2

The basic technical and operational data of a Buckau-Wolf R8VD-136 Engine.

Parameter	Description
Number of cylinders	8
Cylinder bore	240 mm
Piston stroke	360 mm
Cylinder working volume	16.290 dm ³
Compression chamber volume	1.205 dm ³
Nominal effective power	300 HP (220 kW)
Nominal speed	360 rpm
Compression ratio	14.4
Nominal mean effective pressure	5.75 bar (0.575 MPa)
Maximum combustion pressure	52 bar (5.2 MPa)
Compression pressure	36 bar (3.6 MPa)
Mean piston speed	4.32 m/s
Nominal specific fuel oil consumption	175 ± 18 g/HPH (238 ± 24 g/kWh)
Dry engine mass	8500 kg
Equipment mass	1000 kg

2. Basic polyharmonic model calculation code

```
% polyharmonic.m
clear,clc,close all
FF = [731.615 727.478 737.458 758.88 786.004 811.566
      828.719 832.865 822.89 801.465 774.332 748.764 731.615
      727.478 737.458 758.88 786.004 811.566 828.719 832.865
      822.89 801.465 774.332 748.764 731.615
      988.499 1005.43 989.138 943.975 882.046 819.94 774.299
      757.354 773.648 818.819 880.757 942.865 988.499
      1005.43 989.138 943.975 882.046 819.94 774.299 757.353
      773.649 818.819 880.757 942.864 988.499
      871.124 823.759 822.936 868.881 949.282 1042.6 1123.82
      1171.18 1172 1126.05 1045.65 952.341 871.124 823.758
      822.937 868.881 949.282 1042.6 1123.82 1171.19 1172
      1126.05 1045.65 952.341 871.124
      1166.33 1237.24 1253.23 1210.01 1119.16 1005.03 898.194
      827.286 811.302 854.525 945.373 1059.5 1166.33 1237.24
      1253.23 1210.01 1119.16 1005.03 898.194 827.285
```

Basic polyharmonic model calculation code (continued)

```
% polyharmonic.m
811.302 854.525 945.373 1059.5 1166.33
847.885 796.422 795.302 844.823 931.716 1032.7 1120.71
1172.17 1173.29 1123.77 1036.88 935.898 847.885
796.422 795.302 844.823 931.716 1032.7 1120.71 1172.17
1173.29 1123.77 1036.88 935.899 847.885
1093.01 1123.7 1108.89 1052.54 969.753 882.713 814.743
784.052 798.867 855.215 938.001 1025.04 1093.01 1123.7
1108.89 1052.54 969.753 882.713 814.743 784.053
798.867 855.216 938.001 1025.04 1093.01
852.035 799.741 797.223 845.152 930.689 1030.91 1118.97
1171.26 1173.78 1125.85 1040.31 940.09 852.035 799.742
797.222 845.152 930.689 1030.91 1118.97 1171.26
1173.78 1125.85 1040.31 940.09 852.035
1142.22 1212.93 1231.62 1193.29 1108.2 999.16 895.38
824.67 805.978 844.311 929.399 1038.44 1142.22 1212.93
1231.62 1193.29 1108.2 999.16 895.38 824.67 805.977
844.311 929.399 1038.44 1142.22
988.146 944.118 933.953 960.373 1016.3 1086.75 1152.84
1196.87 1207.04 1180.62 1124.69 1054.24 988.146
944.118 933.953 960.373 1016.3 1086.75 1152.84 1196.87
1207.04 1180.62 1124.69 1054.24 988.146
603.466 613.507 614.588 606.418 591.187 572.977 556.666
546.624 545.544 553.713 568.944 587.155 603.466
613.507 614.588 606.418 591.187 572.977 556.666
546.624 545.544 553.713 568.944 587.155 603.466];
```

```
[w,N] = size(FF);
path = 'D:\danekn\';
ext = '.jpg';
for k = 1:w % main loop
    close all
    F = FF(k,:); % next journal
    F = F';
    % model A0 + A2*sin(2*fir + fir2)
    fi = [0:15:360]';
    fir = fi*pi/180;% w radianach
    % Application of FFT
    % Analysis
    Widmo = fft(F);
    A = abs(Widmo)*2/N;A(1) = A(1)/2;
    Nmax = 6;
    Faza = pi/2-angle(Widmo(1:Nmax + 1));
    if k==1
        model02 = [k*ones(Nmax + 1,1),[0:Nmax]',A(1:Nmax +
        1),Faza'*180/pi];
    else
        model02 = [model02;[k*ones(Nmax + 1,1),[0:Nmax]',A(1:
        Nmax + 1),Faza'*180/pi]];
    end % if
    figure(2)
    subplot(2,1,1)
    stem([0:Nmax],A(1:Nmax + 1),'ro'),grid on
    ylabel('Amplitude (N)'),xlabel('Harmonic (-)')
    title(strcat('Journal no. ',num2str(k)))
    subplot(2,1,2)
    stem([0:Nmax],Faza(1:Nmax + 1)*180/pi,'ro'),grid on
    ylabel('Phase (deg)'),xlabel('Harmonic (-)')
    filename = strcat(path,'pic_',num2str(k),'_2',ext);
    % zapis figure(2)
    saveas(gcf,filename,'jpg')
    % Syntesis
```

```

model_poli = A(1)*ones(N,1);
for K = 2:Nmax + 1
    model_poli = model_poli + A(K)*sin((K-1)*fir + Faza(K));
end % for K
figure(3)
D2 = F-model_poli;
q2 = sum(abs(D2))/N;
if k==1,Q2 = q2;else Q2 = [Q2;q2];end
plot(fir,F,'b-o',fir,model_poli,'r+-',fir,q2,'ko-')
legend('FEA calculation','Poliharmonic model','\Delta','Location','Best'),grid on
title(strcat('Journal no. ',num2str(k)))
filename = strcat(path,'pic_',num2str(k),'_3',ext);
% zapis figure(3)
saveas(gcf,filename,'jpg')
end % for k
disp('Poliharmonic model')
disp('Journal Harmonic Amplitude (N) Phase (deg)')
disp(model02)

```

3. Spline-based polyharmonic model calculation code

```

%splines.m
clear,clc
G = [731.615 727.478 737.458 758.88 786.004 811.566
828.719 832.865 822.89 801.465 774.332 748.764 731.615
727.478 737.458 758.88 786.004 811.566 828.719 832.865
822.89 801.465 774.332 748.764 731.615
988.499 1005.43 989.138 943.975 882.046 819.94 774.299
757.354 773.648 818.819 880.757 942.865 988.499
1005.43 989.138 943.975 882.046 819.94 774.299 757.353
773.649 818.819 880.757 942.864 988.499
871.124 823.759 822.936 868.881 949.282 1042.6 1123.82
1171.18 1172 1126.05 1045.65 952.341 871.124 823.758
822.937 868.881 949.282 1042.6 1123.82 1171.19 1172
1126.05 1045.65 952.341 871.124
1166.33 1237.24 1253.23 1210.01 1119.16 1005.03 898.194
827.286 811.302 854.525 945.373 1059.5 1166.33 1237.24
1253.23 1210.01 1119.16 1005.03 898.194 827.285
811.302 854.525 945.373 1059.5 1166.33
847.885 796.422 795.302 844.823 931.716 1032.7 1120.71
1172.17 1173.29 1123.77 1036.88 935.898 847.885
796.422 795.302 844.823 931.716 1032.7 1120.71 1172.17
1173.29 1123.77 1036.88 935.899 847.885
1093.01 1123.7 1108.89 1052.54 969.753 882.713 814.743
784.052 798.867 855.215 938.001 1025.04 1093.01 1123.7
1108.89 1052.54 969.753 882.713 814.743 784.053
798.867 855.216 938.001 1025.04 1093.01
852.035 799.741 797.223 845.152 930.689 1030.91 1118.97
1171.26 1173.78 1125.85 1040.31 940.09 852.035 799.742
797.222 845.152 930.689 1030.91 1118.97 1171.26
1173.78 1125.85 1040.31 940.09 852.035
1142.22 1212.93 1231.62 1193.29 1108.2 999.16 895.38
824.67 805.978 844.311 929.399 1038.44 1142.22 1212.93
1231.62 1193.29 1108.2 999.16 895.38 824.67 805.977
844.311 929.399 1038.44 1142.22
988.146 944.118 933.953 960.373 1016.3 1086.75 1152.84
1196.87 1207.04 1180.62 1124.69 1054.24 988.146
944.118 933.953 960.373 1016.3 1086.75 1152.84 1196.87
1207.04 1180.62 1124.69 1054.24 988.146
603.466 613.507 614.588 606.418 591.187 572.977 556.666
546.624 545.544 553.713 568.944 587.155 603.466
613.507 614.588 606.418 591.187 572.977 556.666
546.624 545.544 553.713 568.944 587.155 603.466];

```

```

[w,N] = size(G);
fi = [0:15:360];fir = fi*pi/180;
firr = [0:360]*pi/180;
path = 'D:\danekn\';
ext = '.jpg';
for k = 1:10% mail loop
    close all
    F = G(k,:);
    FF = spline(fir,F,firr);
    figure(1)
    plot(fir,F,'bo-',firr,FF,'r:'),grid on
    xlabel('Crank angle (deg)')
    ylabel('Force (N)')
    legend('FEA calculation','Spline interpolstion','Location','Best'),grid on
    title(strcat('Journal no. ',num2str(k)))
    filename = strcat(path,'slide_',num2str(k),'_1',ext);
    % write of figure(1)
    saveas(gcf,filename,'jpg')
    Widmo = fft(FF);
    N = length(FF);
    A = abs(Widmo)*2/N;A(1) = A(1)/2;
    Faza = pi/2-angle(Widmo);
    Nmax = 7;
    figure(2)
    subplot(2,1,1)
    stem([0:Nmax - 1],A(1:Nmax),'ro'),grid on
    title(strcat('Journal no. ',num2str(k)))
    ylabel('Amplitude (N)'),xlabel('Harmonic (-)')
    subplot(2,1,2)
    stem([0:Nmax - 1],Faza(1:Nmax)*180/pi,'ro'),grid on
    ylabel('Phase (deg)'),xlabel('Harmonic (-)')
    filename = strcat(path,'slide_',num2str(k),'_2',ext);
    % write of figure(2)
    saveas(gcf,filename,'jpg')
    % [[0:Nmax-1],A(1:Nmax)'],Faza(1:Nmax)*180/pi]
    Row = [k*ones(Nmax + 1,1),[0:Nmax],A(1:Nmax + 1)'],Faza(1:Nmax + 1)*180/pi];
    if k==1,model03 = Row; else model03 = [model03;Row]; end
    % if
    % Syntesis:
    model_poli = A(1)*ones(1,N);
    for K = 2:Nmax + 1
        model_poli = model_poli + A(K)*sin((K-1)*firr + Faza(K));
    end % for K
    figure(3)
    plot(firr,FF,'b-',firr,model_poli,'r-',firr,FF-model_poli,'k-')
    legend('Spline interpolation','Poliharmonic model','\Delta','Location','Best'),grid on
    title(strcat('Journal no. ',num2str(k)))
    filename = strcat(path,'slide_',num2str(k),'_3',ext);
    % write of figure(3)
    saveas(gcf,filename,'jpg')
    D3 = FF-model_poli;
    q3 = sum(abs(D3))/length(firr);
    if k==1,Q3 = q3;else Q3 = [Q3;q3];end % if
    figure(4)
    plot(firr*180/pi,D3,'k-'),grid on
    xlabel('Crank angle (deg)')
    title(strcat('Journal no. ',num2str(k)))
    ylabel('\Delta')
    filename = strcat(path,'slide_',num2str(k),'_4',ext);
    % zapis figure(4)

```

```

saveas(gcf,filename,'jpg')
end % for k
disp('Journal Harmonic (-) Amplitude (N) Phase (deg)')
disp(model03)
disp('fitting factor Q3:')
Q3 = [[1:10],Q3];
disp('Journal Q3')
disp(Q3)

```

4. Monoharmonic model calculation code

```

% monoharmonic.m
clear,clc,close all
FF = [731.615 727.478 737.458 758.88 786.004 811.566
      828.719 832.865 822.89 801.465 774.332 748.764 731.615
      727.478 737.458 758.88 786.004 811.566 828.719 832.865
      822.89 801.465 774.332 748.764 731.615
      988.499 1005.43 989.138 943.975 882.046 819.94 774.299
      757.354 773.648 818.819 880.757 942.865 988.499
      1005.43 989.138 943.975 882.046 819.94 774.299 757.353
      773.649 818.819 880.757 942.864 988.499
      871.124 823.759 822.936 868.881 949.282 1042.6 1123.82
      1171.18 1172 1126.05 1045.65 952.341 871.124 823.758
      822.937 868.881 949.282 1042.6 1123.82 1171.19 1172
      1126.05 1045.65 952.341 871.124
      1166.33 1237.24 1253.23 1210.01 1119.16 1005.03 898.194
      827.286 811.302 854.525 945.373 1059.5 1166.33 1237.24
      1253.23 1210.01 1119.16 1005.03 898.194 827.285
      811.302 854.525 945.373 1059.5 1166.33
      847.885 796.422 795.302 844.823 931.716 1032.7 1120.71
      1172.17 1173.29 1123.77 1036.88 935.898 847.885
      796.422 795.302 844.823 931.716 1032.7 1120.71 1172.17
      1173.29 1123.77 1036.88 935.899 847.885
      1093.01 1123.7 1108.89 1052.54 969.753 882.713 814.743
      784.052 798.867 855.215 938.001 1025.04 1093.01 1123.7
      1108.89 1052.54 969.753 882.713 814.743 784.053
      798.867 855.216 938.001 1025.04 1093.01
      852.035 799.741 797.223 845.152 930.689 1030.91 1118.97
      1171.26 1173.78 1125.85 1040.31 940.09 852.035 799.742
      797.222 845.152 930.689 1030.91 1118.97 1171.26
      1173.78 1125.85 1040.31 940.09 852.035
      1142.22 1212.93 1231.62 1193.29 1108.2 999.16 895.38
      824.67 805.978 844.311 929.399 1038.44 1142.22 1212.93
      1231.62 1193.29 1108.2 999.16 895.38 824.67 805.977
      844.311 929.399 1038.44 1142.22
      988.146 944.118 933.953 960.373 1016.3 1086.75 1152.84
      1196.87 1207.04 1180.62 1124.69 1054.24 988.146
      944.118 933.953 960.373 1016.3 1086.75 1152.84 1196.87
      1207.04 1180.62 1124.69 1054.24 988.146
      603.466 613.507 614.588 606.418 591.187 572.977 556.666
      546.624 545.544 553.713 568.944 587.155 603.466
      613.507 614.588 606.418 591.187 572.977 556.666
      546.624 545.544 553.713 568.944 587.155 603.466];

```

```

[w,N] = size(FF);
path = 'D:\danekn\';
ext = '.jpg';
for k = 1:w % main loop
    close all
    F = FF(k,:); % next journal
    F = F';
    % model A0 + A2*sin(2*fir + fir2)
    fi = [0:15:360]';
    fir = fi*pi/180;% in radians

```

```

A0 = mean(F);% constant component
amin = min(F);
amax = max(F);
A2 = (amax - amin)/2;% Amplitude of 2nd harmonic
%phase of 2nd harmonic
fir2 = asin((F(1) - A0)/A2);
if fir2 < 0,fir2 = fir2+(3*pi/2);end % correction for fir2 < 0
model = A0 + A2*sin(2*fir + fir2);
figure(1),plot(fi,F,bo-',fi,model,'r*-',fi,F-model,'ko-')
legend('FEA calculation','2nd harmonic model','\Delta','Loca
tion','Best')
grid on
title(strcat('Journal no. ',num2str(k)))
filename = strcat(path,'pic_',num2str(k),'_1',ext);
format bank
D1 = F-model;
q1 = sum(abs(D1))/N;
if k==1,model01 = [k,A0,A2,fir2*180/pi,q1];Q1 = q1;
    else model01 = [model01;[k,A0,A2,fir2*180/pi,q1]];Q1 = [Q1;
    q1];
end % if
xlabel('Crank angle (deg)')
ylabel(strcat('Force(N)',num2str(k),'));
% write figure(1)
saveas(gcf,filename,'jpg')
end % for k
disp('Monoharmonic model')
disp('Journal A0 A2 Phase [deg] Q1')
disp(model01)

```

References

- [1] L. Chybowski, K. Gawdzińska, R. Laskowski, Assessing the unreliability of systems during the early operation period of a ship – a case study, *J. Mar. Sci. Eng.* 7 (213) (2019) 1–12, <https://doi.org/10.3390/jmse7070213>.
- [2] Z. Łukowski, *Technologia spalinowa silników kolejowych i okrętowych [Exhaust gas technology of railway and marine engines]*, WKiŁ, Warsaw, 1972.
- [3] K. Gawdzińska, L. Chybowski, W. Przetakiewicz, R. Laskowski, Application of FMEA in the quality estimation of metal matrix composite castings produced by squeeze infiltration, *Arch. Metall. Mater.* 62 (2017) 2171–2182, <https://doi.org/10.1515/amm-2017-0320>.
- [4] K. Gawdzińska, L. Chybowski, W. Przetakiewicz, Study of thermal properties of cast metal-ceramic composite foams, *Arch. Foundry Eng.* 17 (2017) 47–50.
- [5] K. Gawdzińska, L. Chybowski, W. Przetakiewicz, Proper matrix-reinforcement bonding in cast metal matrix composites as a factor of their good quality, *Arch. Civ. Mech. Eng.* (2015), <https://doi.org/10.1016/j.acme.2015.11.004>.
- [6] K. Nozdrzykowski, Ł. Nozdrzykowski, New conception of evaluation the geometrical state and bearing of extralarge crankshafts, *Przegląd Elektrotechniczny*. 1 (2017) 105–108, <https://doi.org/10.15199/48.2017.09.21>.
- [7] K. Nozdrzykowski, D. Janecki, Comparative studies of reference measurements of cylindrical surface roundness profiles of large machine components, *Metrol. Meas. Syst.* XX 1 (2014) 67–76.
- [8] K. Nozdrzykowski, Adjustment and analysis of forces in a flexible crankshaft support system, *J. Mach. Constr. Maintance, Probl. Eksploat.* 4 (2017) 63–70.
- [9] U. Barth, Kombinierte Zweipunkt – Dreipunkt – Messung zum gleichzeitigen Bestimmen von Mass – Kreisformabweichungen, *Feingerätetechnik*. 1 (1984) 21–23.
- [10] D. Diakov, I. Kalimanova, T. Minakov, System for measurements of roundness of large scaled objects, in: *Konf. Nauk. Metrol. w Tech. Wytw.*, Cracow University of Technology, Cracow, 2003, pp. 121–128.
- [11] T.R. Nyberg, M. Kotamaki, Cylindricity measurement of large rollers by combined 3-point-method and sequential 2-point-method, in: *4th Int. Symp. Dimens. Metrol. Prod. Quality Control*, 22–25 June 1992, Tampere, Finland, 1992: Paper no 16.
- [12] S. Adamczak, Odniesieniowe metody pomiaru zarysów okrągłości części maszyn [Reference methods for measuring the roundness profiles of machine parts], *Kielce University of Technology*, Kielce, 1998.
- [13] S. Sonozaki, H. Fujiwara, Simultaneous measurement of cylindrical parts profile and rotating accuracy using multi-three-point-method, *Japan. Soc. Prec. Eng.* (1989) 286–291.
- [14] E. Westkamper, Prozessnahe Rundheitsmesstechnik mit 3-Punktmesssystemen, in: *6-Th Int. DAAAM Symp. Proc.*, Cracow, 1995, pp. 363–364.

- [15] E. Okuyama, K. Goho, K. Mitsui, New analytical method for V-block three-point method, *Precis. Eng.* 27 (2003) 234–244, [https://doi.org/10.1016/S0141-6359\(03\)00002-3](https://doi.org/10.1016/S0141-6359(03)00002-3).
- [16] W.Q. Zhao, Z. Xue, J.B. Tan, Z.B. Wang, SSEST: A new approach to higher accuracy cylindricity measuring instrument, *Int. J. Mach. Tools Manuf.* 46 (2006) 1869–1878, <https://doi.org/10.1016/j.ijmachtools.2005.11.006>.
- [17] W. Gao, S. Kiyono, On-machine roundness measurement of cylindrical workpieces by the combined three-point method, *Measurement* 21 (1997) 147–156, [https://doi.org/10.1016/S0263-2241\(97\)00060-2](https://doi.org/10.1016/S0263-2241(97)00060-2).
- [18] Y.-Z. Lao, H.-W. Leong, F.P. Preparata, G. Singh, Accurate cylindricity evaluation with axis-estimation preprocessing, *Precis. Eng.* 27 (2003) 429–437, [https://doi.org/10.1016/S0141-6359\(03\)00044-8](https://doi.org/10.1016/S0141-6359(03)00044-8).
- [19] B. Muralikrishnan, S. Venkatachalam, J. Raja, M. Malburg, A note on the three-point method for roundness measurement, *Precis. Eng.* 29 (2005) 257–260, <https://doi.org/10.1016/j.precisioneng.2004.06.007>.
- [20] HHI, Technical materials of HHI Co., Ltd., South Korea, 2018.
- [21] HCP, Shape and position tolerances of crankshafts – Engine technology specification MAN, H. Cegielski S.A., Poznań, 2010.
- [22] M. Moghtaderi, Diesel Engine Crankshaft Deflection Measurement, 07.07.2015. <https://www.linkedin.com/pulse/diesel-engine-crankshaft-deflection-measurement-mahmoud-moghtaderi/>, 2015 (accessed August 28, 2019).
- [23] D. Janecki, K. Stępień, S. Adamczak, Investigating methods of mathematical modelling of measurement and analysis of spherical surfaces, in: *Proc. X Int. Symp. Meas. Qual. Control–ISMQC 2010*, Osaka, 2010, pp. 1–4.
- [24] K. Nozdrzykowski, Prevention of elastic strains in flexible large size machine parts with the use of elastic support, *Mach. Dyn. Res.* 39 (2015) 111–122.
- [25] K. Nozdrzykowski, Method and apparatus for measuring deviations in the shape and position of crankshaft pins axes, PL218653, 2011.
- [26] K. Nozdrzykowski, Z. Grządziel, J. Harušinec, Determining and analysing support conditions at variable construction of crankshafts, *New Trends Prod. Eng.* 1 (2018) 553–560, <https://doi.org/10.2478/ntpe-2018-0069>.
- [27] K. Nozdrzykowski, L. Chybowski, A force-sensor-based method to eliminate deformation of large crankshafts during measurements of their geometric condition, *Sensors* 19 (2019) 3507, <https://doi.org/10.3390/s19163507>.
- [28] L. Chybowski, Z. Grządziel, K. Gawdzińska, Simulation and experimental studies of a multi-tubular floating sea wave damper, *Energies* 11 (2018) 1012, <https://doi.org/10.3390/en11041012>.
- [29] K. Nozdrzykowski, Procedures of determining and realization of reaction forces in an elastic support system for crankshafts, *Mechanik* (2018) 1129–1131.
- [30] PRS, Calculation of crankshafts for marine diesel engines, Polish Register of Shipping, Gdańsk, 2012.
- [31] K. Summerhays, R. Henke, J. Baldwin, R. Cassou, C. Brown, Optimizing discrete point sample patterns and measurement data analysis on internal cylindrical surfaces with systematic form deviations, *Precis. Eng.* 26 (2002) 105–121, [https://doi.org/10.1016/S0141-6359\(01\)00106-4](https://doi.org/10.1016/S0141-6359(01)00106-4).
- [32] S. Adamczak, D. Janecki, K. Stępień, Problems of mathematical modelling of rotary elements, in: *Proc. Int. Symp. Prod. Res. 2018*, Springer International Publishing, Cham, 2019, pp. 747–752, doi: 10.1007/978-3-319-92267-6_60.
- [33] K. Nozdrzykowski, Applying harmonic analysis in the measurements of geometrical deviations of the crankshafts – selecting support conditions, *MAPE 1* (2018) 191–195, <https://doi.org/10.2478/mape-2018-0025>.
- [34] E. Capello, Q. Semeraro, The harmonic fitting method for the assessment of the substitute geometry estimate error. Part I: 2D and 3D theory, *Int. J. Mach. Tools Manuf.* 41 (2001) 1071–1102, [https://doi.org/10.1016/S0890-6955\(01\)00019-0](https://doi.org/10.1016/S0890-6955(01)00019-0).
- [35] A. Bejger, L. Chybowski, K. Gawdzińska, Utilising elastic waves of acoustic emission to assess the condition of spray nozzles in a marine diesel engine, *J. Mar. Eng. Technol.* (2018), <https://doi.org/10.1080/20464177.2018.1492361>.
- [36] M. Heideman, D. Johnson, C. Burrus, Gauss and the history of the fast Fourier transform, *IEEE ASSP Mag.* 1 (1984) 14–21, <https://doi.org/10.1109/MASSP.1984.1162257>.
- [37] M.J. Mohlenkamp, A fast transform for spherical harmonics, *J. Fourier Anal. Appl.* 5 (1999) 159–184, <https://doi.org/10.1007/BF01261607>.
- [38] S. Kunis, D. Potts, Fast spherical Fourier algorithms, *J. Comput. Appl. Math.* 161 (2003) 75–98, [https://doi.org/10.1016/S0377-0427\(03\)00546-6](https://doi.org/10.1016/S0377-0427(03)00546-6).
- [39] L. Dorobczyński, J. Brzózka, *MATLAB środowisko obliczeń naukowo-technicznych*, I, PWN, Warsaw, 2008.
- [40] C.A. Hall, W.W. Meyer, Optimal error bounds for cubic spline interpolation, *J. Approx. Theory.* 16 (1976) 105–122, [https://doi.org/10.1016/0021-9045\(76\)90040-X](https://doi.org/10.1016/0021-9045(76)90040-X).
- [41] I.N. Bronshtein, K.A. Semendyaev, G. Musiol, H. Mühlig, *Handbook of Mathematics*, Springer-Verlag, Berlin Heidelberg, Frankfurt, 2015.